New investigation of the neutron-neutron and neutron-proton final-state interaction in the *n-d* breakup reaction

V. Huhn,* L. Wätzold, Ch. Weber,† A. Siepe, and W. von Witsch‡
Institut für Strahlen- und Kernphysik, Universität Bonn, D-53115 Bonn, Germany

H. Witała
Institute of Physics, Jagellonian University, Reymonta 4, PL-30059 Cracow, Poland

W. Glöckle
Institut für Theoretische Physik II, Ruhr-Universität Bochum, D-44780 Bochum, Germany

(Received 14 August 2000; published 15 December 2000)

The neutron-neutron final-state interaction (FSI) has been investigated in the ^{2}H$(n,np)n$ reaction at 25.3 and 16.6 MeV, detecting neutrons and protons in coincidence in a geometry which should enable a practically model-independent determination of the $^1S_0$ neutron-neutron scattering length a_{nn}. The analysis was performed by means of detailed Monte Carlo simulations based on rigorous three-body calculations with realistic nucleon-nucleon potentials. At 25.3 MeV, the value of a_{nn} deduced from the absolute cross section in the FSI peak is -16.3 ± 0.4 fm while the relative cross section, normalized in the region of neutron-proton quasifree scattering, gives -16.1 ± 0.4 fm. The relative data obtained at 16.6 MeV yielded $a_{nn}=-16.2\pm0.3$ fm. In addition, the $^1S_0$ neutron-proton scattering length was measured at 25.2 MeV in the same configuration for comparison. While our results for a_{nn} are incompatible with those of a similar investigation performed recently at 13 MeV where the two neutrons were detected, both results for a_{np} are in good agreement with the accurately known value from free *n-p* scattering.

DOI: 10.1103/PhysRevC.63.014003 PACS number(s): 13.75.Cs, 21.45.+v, 25.10.+s

I. INTRODUCTION

From the early days of nuclear physics, the effective range theory has been an important tool in the quest for a better understanding of the interaction between nucleons. Especially the $^1S_0$ nucleon-nucleon (*NN*) scattering length a_{NN} is a powerful magnifying glass to study the *NN* interaction. Because the $^1S_0$ state is almost bound, the scattering length has a large negative value, and small changes in the depth and width of a two-nucleon potential cause large changes in a_{NN}. The neutron-neutron and proton-proton scattering lengths a_{nn} and a_{pp} are of special interest because, in principle, they allow a very sensitive test of charge symmetry in the strong interaction [1]. However, charge symmetry breaking, which is due to the difference between the *u* and *d* quarks, is a small effect [2], and accurate values of the scattering lengths are needed for a quantitative evaluation. While a_{pp} can be measured very accurately via *p-p* scattering, large and model-dependent corrections are necessary in order to obtain the nuclear part of this scattering length, a_{pp}^N. In the case of a_{nn}, these corrections are much smaller but the measurement is more difficult because one must resort to multiparticle breakup reactions with two neutrons in the exit channel.

Numerous attempts [3,4] have been made in more than 35 years to determine a_{nn}, using mostly the ^{2}H$(\pi^-,nn)\gamma$ and ^{2}H$(n,nn)p$ reactions and investigating the region of the *n-n* final-state interaction (FSI) where the two neutrons travel together with small relative energy. By 1990, the situation could be summarized as follows [2,5]. The ^{2}H$(\pi^-,nn)\gamma$ reaction provided an average of $a_{nn}=-18.6\pm0.5$ fm, and the results obtained with neutron-induced breakup experiments fell into two distinct groups: while the kinematically complete experiments consistently yielded values around -16.5 fm, the average result from the kinematically incomplete ones was -19.0 fm. However, the majority of the *n*-induced breakup experiments till then had been analyzed by means of a simple Watson-Migdal [6] parametrization or, at best, with Faddeev-type calculations using simplified, finite-rank forces for the *NN* interaction. In the meantime, most of the kinematically *incomplete* experiments have been reanalyzed [7] with rigorous three-nucleon ($3N$) calculations [8] based on realistic *NN* potentials—with strikingly different results, which now clustered around -15.5 fm. It became clear that in kinematically incomplete experiments the result depends strongly on the *NN* force used in the calculations while in kinematically complete ones the *shape* of the FSI enhancement, i.e., the width of the peak, is not sensitive to the details of the *NN* interaction but is determined solely by the value of a_{nn}. In fact, it was shown by Glöckle *et al.* [8] that, in kinematically complete breakup experiments, using the Watson-Migdal formalism to fit the shape of the FSI peak produces results for a_{nn} which do not differ by more than 0.5 fm from those obtained with modern, dynamically exact $3N$ calculations. However, even after such calculations became feasible one problem still remained, namely the possible in-

*Present address: Deutsche Telekom MobilNet GmbH, D-53184 Bonn, Germany.
†Present address: Mannesmann Arcor AG & Co., D-65760 Eschborn, Germany.
‡Electronic address: vwitsch@iskp.uni-bonn.de

fluence of three-body forces (3BF), whose theoretical foundation is still in its infancy. Consequently, up to then only the results from the $^2\mathrm{H}(\pi^-,nn)\gamma$ reaction were taken seriously while those obtained with neutron-induced reactions were all but rejected.

This situation changed when Witala *et al.* [9] found that, in kinematically *complete* *n-d* experiments, the cross section in the FSI peak becomes practically independent of the *NN* potential for specific production angles of the *N-N* pair and, more importantly, also the influence of three-body forces appears to vanish. Although the reason for this insensitivity is not yet understood, it now made kinematically complete *n-d* breakup experiments, performed at these angles, especially promising because they should enable a virtually model-independent determination of a_{nn}. A first experiment of that kind, done at $E_0=13$ MeV, has been described recently [10]. In the present paper we report on a similar investigation at 25.3 and 16.6 MeV, and employing a different geometry.

II. EXPERIMENTAL DETAILS

A. Kinematics

In most previous *n-d* experiments aimed at the determination of a_{nn} a thick, active target was used and the two neutrons were detected with two scintillators positioned close to each other at the same (or nearly the same) angle on one side of the beam (in the following called ''final-state'' geometry). Such an arrangement yields a clean kinematical condition for the observation of the *n-n* FSI but it produces strong cross talk between the two detectors, which is a serious source of background. In the present experiment, we have avoided this problem by detecting only one of the neutrons in coincidence with the recoiling proton on the opposite side of the beam (''recoil'' geometry). Although this mandated the use of a thin target foil since both the neutron and the proton must be detected at well-defined angles, the smaller target thickness was compensated by the use of a higher beam intensity, by the 100% efficiency of the proton detector, and by a higher cross section. Also, there were no losses or distortions due to neutron multiple scattering in the target, and less background. The main advantage of this geometry, however, is the simultaneous observation of quasifree *n-p* scattering (QFS) where the cross section is virtually independent of the *n-n* scattering length and thus provides a convenient, built-in normalization for the *n-n* FSI peak. The kinematical situation is illustrated in Fig. 1. The neutrons were detected at $\Theta_n=55.5°$ and the protons at $\Theta_p=41.15°$, with $\Phi_{np}=180°$, which are the ''magic'' angles at which the model dependency of the breakup cross section vanishes at 25.3 MeV [9]. Since the *n-n* FSI occurs at high proton energies and runs nearly parallel to the E_n axis, a relatively thick target could be used nevertheless and, by projecting the *n-p* coincidences onto the E_n axis, the energy smearing in the proton arm does not affect the resolution in the FSI peak. In addition, the low neutron energies in the *n-n* FSI peak ensure a good time-of-flight (TOF) resolution even at a fairly small distance between the target and the *n* detector. Due to the rather large target thickness the *n-p* FSI, which occurs at low proton energies, could not be observed in the actual data of this experiment. However, if the *p* detector is replaced by another *n* detector the *n-p* FSI occurs in place of the *n-n* FSI, and the accurately known *n-p* scattering length can be measured in the *same geometry* for comparison, providing a test for the reliability of the method.

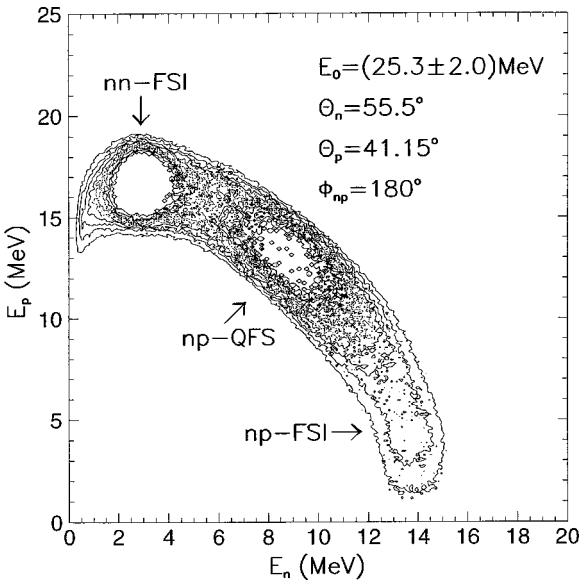

FIG. 1. Finite-geometry Monte Carlo simulation of the kinematical locus for the $^2\mathrm{H}(n,np)n$ reaction, with central laboratory angles $\Theta_n=55.5°$, $\Theta_p=41.15°$, and $\Theta_{np}=180°$, at $23.3\leqslant E_0\leqslant 27.3$ MeV. The energy loss of the protons is not included in this simulation; in the actual data the *n-p* FSI cannot be seen in this reaction because the proton energies are too low.

B. Experimental setup

The experiment was performed at the cyclotron of the Institut für Strahlen-und Kernphysik at the University of Bonn. In contrast to our previous experiment [11], a quasi-monoenergetic neutron beam was used this time, and absolute cross sections were measured. A plan view of the experimental layout for the measurement of a_{nn} is shown in Fig. 2. The neutron beam was produced via the $^2\mathrm{H}(d,n)^3\mathrm{He}$ reaction with 26.9-MeV deuterons incident on a 47-mm-long, liquid-nitrogen-cooled gas target, operated at a pressure of 39 bars. With a deuteron beam intensity of 900 nA, the average effective gas density in the beam was typically 77% of the density without beam. The primary beam was stopped directly behind the gas target which served as a Faraday cup. The neutrons were collimated at 0° in a 120-cm-long W-Cu collimator to form a well-defined [12] circular beam with a diameter of 31 mm [full width at half maximum (FWHM)] at the reaction target which was positioned 195 cm from the center of the gas target. The neutron flux on the target in the quasimonoenergetic high-energy (HE) peak from the $^2\mathrm{H}(d,n)^3\mathrm{He}$ reaction was $3.7\times10^5/\mathrm{s\,cm^2}$, with an average energy $E_0=25.3$ MeV and an energy spread $\Delta E_0=4.0$ MeV. The HE neutrons could be separated cleanly from the lower-energy (LE) breakup continuum of the $^2\mathrm{H}(d,n)pd$ reaction by their time of flight. As a beam monitor, a double proton-recoil telescope (PRT) was placed in the

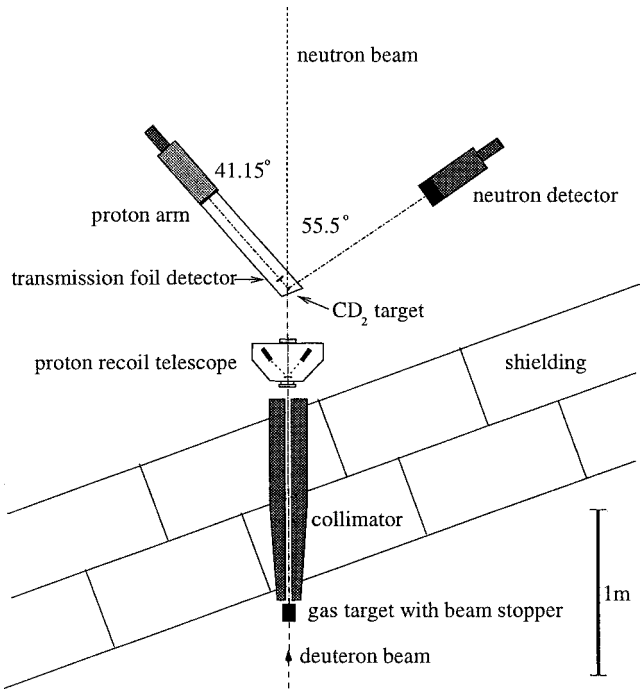

FIG. 2. Schematic drawing of the experimental setup for the a_{nn} measurement, approximately to scale. For the investigation of the *n-p* FSI via the ^{2}H$(n,nn)p$ reaction, the proton arm was replaced by a second neutron detector, positioned at the same angle.

n beam 148 cm from the gas target to detect protons emitted from a 24-mg/cm^2-thick CH_2 target at angles of $\pm 35°$ with respect to the *n* beam. The two telescopes, which were housed in a scattering chamber equipped with 100-μm-thick Be entrance and exit windows, each consisted of a Si surface barrier ΔE and a CsI(T1) *E* detector. In the PRT, too, the HE and LE parts of the spectrum were well separated from each other. As described in the next section, the PRT was essential for the absolute normalization of the HE neutron beam. In addition, it enabled the exact determination of the effective thickness of the gas target, needed to calculate the energy spread of the beam.

For the a_{nn} measurement, the reaction target was a deuterated polyethylene foil with a thickness of 48 mg/cm^2, suspended in an Al frame by means of two thin (0.1 mm) Be wires. It had an elliptical shape and was oriented such that it faced the proton detector, thereby appearing to the neutron beam as a circular disc with 22-mm diameter. Thus the recoil protons suffered minimal energy loss in the target while multiple scattering for the breakup neutrons remained very small. At the position of the CD_2 target, the *n* beam had a plateau of constant intensity with a diameter of >25 mm [12] so that the whole target was illuminated homogeneously. At a distance of 8 cm from the target and outside of the neutron beam, an NE104 scintillator foil of 4.7 mg/cm^2 thickness was positioned in a wedge-shaped Al reflector equipped with thin (5 μm) entrance and exit foils, viewed from above by an RCA 8850 photomultiplier. The charged-particle signals produced in this transmission foil detector (TFD) were used as start signals for all TOF measurements. The protons were detected with an NE104 plastic scintillator of 10-cm diameter and 5-mm thickness, positioned 70 cm from the CD_2 target and viewed by a 5-in. photomultiplier. The face of the scintillator was vapor-coated with a thin layer of Al to prevent any cross talk with the TFD. The target and transmission detector were mounted in an evacuated pipe, in the following called ''proton arm,'' which was sealed at the front end with a 100-μm-thick Be entrance window and a 30-μm Ti exit foil for the *n* beam. At the far end it was closed by the *p*-detector scintillator. Beryllium was used because of its negative *Q* values for the (*n,p*) and (*n,pn*) reactions.

The *n* detector was positioned at a distance of 100 cm from the CD_2 target on the opposite side of the beam. It consisted of a standard BA1 cell filled with NE213 liquid scintillator [13]. It had a nominal diameter of 5 in. and a thickness of 3 in., and was equipped with *n*-γ pulse-shape discrimination [14]. From the specifications of the supplier and from our own measurements (performed with an identical cell which was opened up and measured after it had developed a leak) we assess the uncertainty in the inner diameter of the scintillator vessel at ± 0.5 mm, corresponding to an error of 0.8% in the solid angle subtended by the detector. All detectors were unshielded and surveyed to a precision of $<0.05°$. They were provided with LED pulsers to monitor gain shifts and dead times as well as other effects caused by high count rates, like pileup and distortions in the TOF spectra.

For the measurement of a_{np}, the proton arm was replaced by a second *n* detector of equal size, also placed at 100 cm from the target which now consisted of a thin-walled (0.1 mm), upright Al cylinder, 65 mm high and 44 mm in diameter. It was filled to a height of 60 mm with C_6D_{12} liquid scintillator (BC539 [15]), closed at the bottom with a quartz window and viewed from below by a 2-in. photomultiplier.

The zero points of the time scales in the two detector arms were determined using coincident γ rays from a ^{22}Na source; they were adjusted to lie in the middle of the time scales. During the experiment, an additional time calibration was provided by the prompt γ peaks appearing in the TOF spectra of the two detectors. The timing in both arms was investigated also as a function of pulse height, again using a ^{22}Na source, so that any remaining time walk could be corrected in the offline analysis. The time resolution was typically 0.9 ns for all detectors.

C. Neutron beam calibration

Because absolute cross sections were to be measured with high precision, the neutron fluence F_n, i.e., the number of neutrons/cm^2 at the position of the target, had to be known accurately. This was accomplished by means of *n-p* scattering. Neutron-proton scattering was used because, at angles around $\Theta_{\text{c.m.}}=90°$, the differential cross section is mainly determined by the *S*-wave phase shifts which are known very accurately from precise total cross section data so that we may assume an error of 0.8% for the differential cross section. In fact, the predictions for $d\sigma/d\Omega(90°)$ of the most recent *n-p* phase-shift analyses (PSA) by Stoks *et al.* [16] and by Arndt *et al.* [17], as well as the results of modern,

realistic *NN* potentials [18–20], all agree within 0.4%. In contrast, the uncertainty in the cross section for elastic *n-d* scattering is considerably larger.

To determine F_n in the intensity plateau for the HE part of the beam, the CD_2 target in the proton arm was replaced by a 10-mg/cm^2 CH_2 foil of equal size. Knowing the number of hydrogen atoms in the target from its weight and chemical composition, and also the *n-p* cross section and the solid angle of the *p* detector, the number of neutrons/cm^2 could be calculated from the number of recoil protons detected. Besides the uncertainty in the *n-p* cross section, the main contributions to the error of F_n came from the uncertainties in the geometry of the experimental setup (0.6%) and from statistics (0.5%), while the subtraction of background contributed 0.3%, resulting in a total experimental error of 0.9%. One source of background was due to protons originating from the Be entrance window and from the carbon in the CH_2 target. Although they generally have lower energies because of the negative *Q* values of the ^{9}Be(n,p) and ^{12}C(n,p) reactions, a few could still fall into the region of elastic *n-p* scattering. Some protons could also reach the detector after scattering from the wall of the vacuum pipe. Both kinds of background were identified by their respective *E*, ΔE, and TOF signals, and corresponding corrections were made.

A second, independent value for F_n was obtained from the simultaneous PRT measurement which had an experimental error of 1.0%. After a small correction of 0.5% for neutron losses due to scattering between the two targets, the fluences measured at the two positions were found to scale with $1/r^2$ within 0.3%, where *r* is the distance from the center of the gas target. Combining these results we conclude that we know the integrated HE neutron flux for the subsequent measurements with the CD_2 target with an absolute accuracy of 1.1%, using the PRT as a relative monitor. A comparable absolute calibration for the LE part of the *n* beam was not feasible. Consequently, only a relative measurement was possible at lower energies, employing the upper part of the LE continuum.

The integrated beam-target luminosity *BT* for the a_{np} measurement was also determined via *n-p* scattering. For this purpose the C_6D_{12} target cylinder was replaced by an identical one filled with C_6H_6 (BC-501A [15]). Scattered neutrons were detected at $\Theta_n = 41°$, and the integrated luminosity was determined relative to the number of counts in the PRT. Actually, the measurement at once provided the product of $(BT \cdot \varepsilon \cdot \Delta\Omega)$, where ε and $\Delta\Omega$ are the efficiency and the solid angle of the *n* detector, respectively. The accuracy of this measurement was 2.1%. In addition, the luminosity was also determined with a detailed Monte Carlo (MC) simulation based on the accurately known value of F_n, in which the attenuation in the collimator wall near the exit was explicitly taken into account. Both results for *BT* agreed within 0.6%, and the overall error for this quantity is 1.2%.

D. Detector efficiencies

The efficiency of the transmission foil detector was determined with the same setup as described above in Sec. II C. By comparing the number of protons counted with and without a coincident TFD signal, the efficiency of the transmission detector was found to be practically 100% for all proton energies.

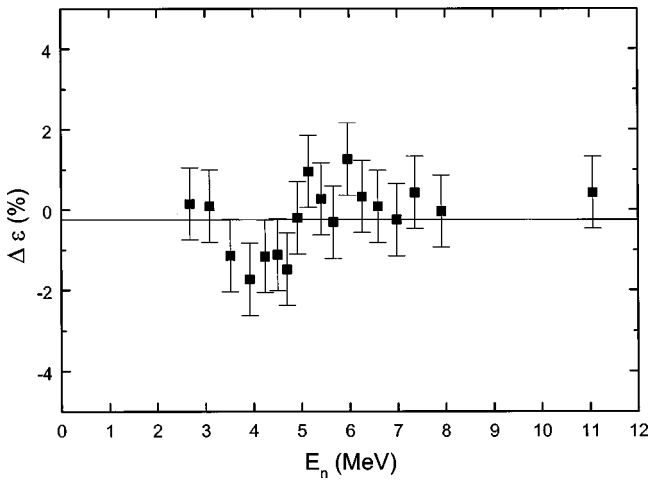

FIG. 3. Measured central efficiency of the neutron detector which was used in the a_{nn} experiment, as a function of E_n, in comparison with the Monte Carlo prediction based on the extended [21] PTB computer code of Dietze and Klein [22]. Shown is the quantity $\Delta\varepsilon = 100\,(\varepsilon_{\rm exp} - \varepsilon_{\rm sim})/\varepsilon_{\rm sim}$ for a dynode threshold of 60 keV ee. The error bars of one standard deviation indicate the total experimental uncertainty.

A special effort went into the accurate determination of the neutron detector efficiencies. Two different and independent methods were used to this end. First, the *central* efficiency was measured, using again the setup with the CH_2 target. The *n* detector was positioned at 90° with respect to the proton arm, close to the target in order to assure that all *n-p* neutrons hit the detector near its center in a narrow cone defined by the solid angle of the *p* detector. The free count rate in the *n* detector was adjusted to be the same as in the *n-d* breakup experiment. For the measurement the whole spectrum of the neutron beam was used, including the continuum from the ^{2}H$(d,n)pd$ reaction. In this way, the efficiency could be determined simultaneously for all energies between $E_n = 2.7$ and 8 MeV, and for 11 MeV using the HE peak of the beam. Windows were set off line in the TOF spectrum of the incoming neutron beam to select bins of energies for the scattered neutrons for which the efficiency was then determined from the number of free proton counts vs the number of *p-n* coincidences. In Figs. 3 and 4, the measured central efficiencies are compared to the results of calculations based on an expanded version [21] of the PTB Monte Carlo efficiency program developed by Dietze and Klein [22]. In the calculations the standard PTB light output function for protons was used, adjusted in scale to reproduce the dynode response spectra which were measured at several neutron energies for each detector. The calculations comprise a complete simulation of the experiment, including the extended geometry and the energy distribution of the incoming neutrons, as well as pileup effects which, at a free count rate of 85 kHz, increased the efficiency on average by 4.1%. The agreement is very good. For detector 1, which was used for the a_{nn} measurement, the average difference between experi-

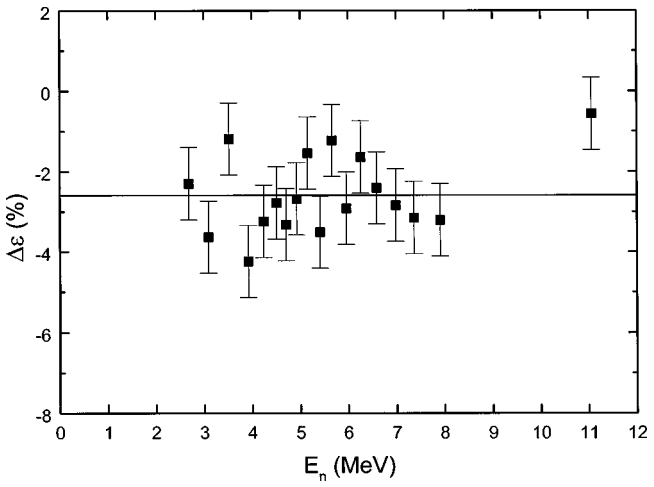

FIG. 4. Same as Fig. 3, but for the second neutron detector.

ment and simulation is 0.2%, with a standard deviation of the data points of $\pm 0.9\%$. The pictures are similar for other detector thresholds, and a trend with energy is not apparent. For the second *n* detector, the difference between prediction and measurement is 2.6%—again without any visible trend in energy.

The main advantages of this measurement are: (i) that the efficiency is determined *in situ*, with the same setup and under virtually the same conditions as those in the breakup experiment and (ii) that it is a relative measurement. No absolute number of neutrons and no absolute cross sections need to be known. It is not even necessary to know the exact value of the detection threshold, as long as it is the same in all measurements. Similarly, neither a possible nonlinearity of the phototube, nor an incorrect proton light-output function or pulse-height resolution affect the accuracy of the experimental result (although they would, of course, sway the outcome of the calculations). Also, beam attenuation form the gas target to the detector is of no concern and, quite important at high count rates, the change in the efficiency due to pileup is automatically included. Therefore, apart from the fact that edge effects were not present here, the results can be applied directly to the breakup experiment. The main error in this efficiency measurement was due to statistics and amounts to $\leqslant 1\%$ per point, except at the highest energy where a small background correction had to be made. Thus we conclude that, in the energy range measured, the renormalized PTB-based calculations reproduce the central efficiency of our *n* detectors within $\pm 0.9\%$.

In order to obtain ε, the *average* efficiency of the detectors as needed for the *n-d* breakup experiments, the PTB program was employed again. According to these calculations, at $E_n = 3$ MeV, e.g., and at a distance of 100 cm between target and detector, the average efficiency is 3.8% smaller than the central one. This is a consequence of three effects, the different geometry being the most important one: as seen from the target, the scintillator is thinner for neutrons impinging close to the edge of the detector which decreases the average efficiency with respect to the central one; this effect can be calculated very accurately. Out scattering near the edge, which can also be calculated reliably, further reduces ε while in scattering from the detector housing increases its value. If we normalize the calculations for each detector to the measured central efficiency, we estimate that the additional error in the calculated average efficiency, coming mainly from the uncertainties in the cross sections for in scattering from the detector housing, is certainly not larger than 1%, resulting in an unparalleled total error of $\pm 1.4\%$. The PTB program also provided the radial dependence of ε which must be taken into account, as will be discussed later.

In addition to the Monte Carlo determination of ε described above, the average efficiencies were also measured directly at four energies in a separate experiment. For this, a small plastic scintillator bar, 10 mm thick and 10 mm high, was suspended in the neutron beam, and neutrons scattered from hydrogen were detected at angles of 70, 60, 50, and 40°, corresponding to the energies $E_{n'} = 3.0$, 6.3, 10.4, and 14.8 MeV, respectively. For each angle, the target bar was oriented perpendicular to the direction of the scattered neutrons, its length being chosen such that the whole target was within the homogeneous part of the neutron beam. This setup assured that the number of recoil protons not being stopped completely in the scintillator as well as multiple scattering for the outgoing neutrons were kept at a minimum. The target was viewed from below by a photomultiplier, dispensing with a light guide in order to minimize the amount of foreign matter in the neutron beam.

Knowing the number of hydrogen atoms in the target scintillator, the *n-p* cross section, the fluence of the neutron beam (see, Sec. II C), and the solid angle $\Delta\Omega_n$ subtended by the *n* detector, the average efficiency could then be obtained from the measured number of *n-p* coincidences, after corrections for background, proton losses and multiple scattering. The results for ε obtained from these measurements agreed with the renormalized PTB predictions within $(1.7 \pm 2.2)\%$, the rather large error being mainly due to background corrections. Thus the outcome of this measurement is compatible with our above results but does not contribute significantly to the accuracy. We therefore assume that we know the average efficiencies of our *n* detectors—for the specific experimental conditions at which they were measured—with an overall uncertainty of $\pm 1.4\%$.

E. Data acquisition and reduction

For the measurement of a_{nn}, the event trigger signal was generated by a fast coincidence between the TFD, the *p* detector, and the *n* detector. For each trigger, eight experimental parameters were written to disc in list mode: the dynode signal as well as (for pulse-shape discrimination purposes) the long and short components of the anode signal from the *n* detector, the dynode signals from the TFD and from the *p* detector, and the TOF's between the TFD and the *n* detector (TOF_n), the *p* detector (TOF_p), and the rf of the cyclotron (TOF_C), respectively. (In the a_{np} measurement, the start signal for all TOF's came from the target scintillator.) In addition, twofold coincidences were recorded between the ΔE and E detectors of the PRT. The trigger signals from the LED pulser driver were counted with a scaler and used to create a separate gate.

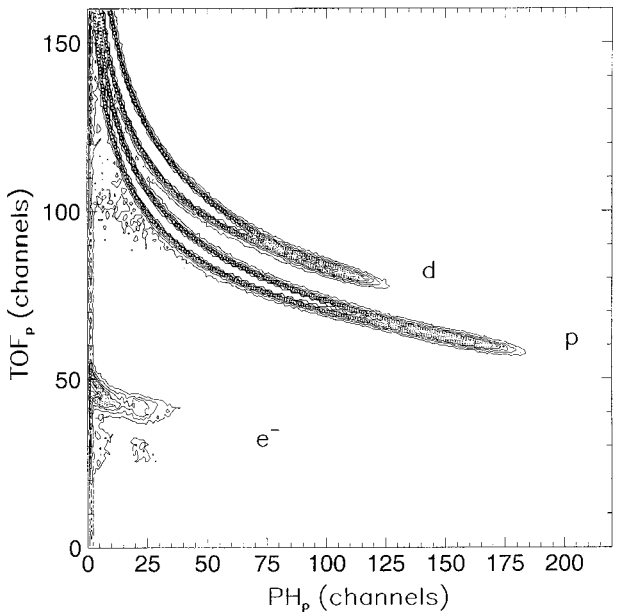

FIG. 5. The matrix (E_p vs TOF$_p$), showing the bands of protons and deuterons, and some events due to electrons which were Compton scattered from the target into the *p* detector.

The total effective running time of the a_{nn} experiment was 400 h, divided into two blocks of 1 week and one block of 2 weeks. The beam intensity was adjusted such as to keep the number of accidentals below 15%. The corresponding singles count rates were 2 kHz in the TFD, 10 kHz in the *p* detector, and 85 kHz in the *n* detector. Special care was taken to limit fluctuations in the count rate of the *n* detector to less than $\pm 6\%$; the data acquisition system was stopped automatically when this limit was exceeded. A background run was made with the CD_2 target replaced by a CH_2 target of equal thickness in order to investigate possible contributions from carbon or hydrogen. (The H_2 contamination in the CD_2 target—measured to be about 1% [11]—could conceivably produce some *n-p* coincidences via multiple scattering. However, no such background was found in the *n-n* FSI region.) The measurement for a_{np} took about 650 h, divided into three separate blocks of 2 weeks each. At a deuteron beam intensity of 100 nA, the singles count rates here were 280 kHz in the target and 15 kHz in the *n* detectors.

The raw data were first reduced by selecting either the HE part of the *n* beam or the upper part of the LE continuum, with an average energy $E_0 = 16.6$ MeV and $\Delta E_0 = 3.0$ MeV (FWHM), using TOF$_C$. A lower threshold equivalent to 60-keV electron energy (keV ee) was set in the dynode spectrum of the *n* detector for the HE data, and 40 keV ee for the LE data. Then, a window was set in the pulse shape matrix to get rid of most coincidences with γ rays in the *n* detector. Coincidences with deuterons or Compton-scattered electrons in the *p* detector were removed by an appropriate window in the (E_p vs TOF$_p$) matrix (Fig. 5). In all cases, conservative windows were used to assure that no true coincidences were lost in the process. The remaining background, being accidental, was subtracted after projection onto the TOF$_n$ axis.

F. Data analysis and corrections

Some corrections had to be applied to the reduced data prior to their comparison with theory. Long-time gain changes in the photomultipliers and possible small shifts of the time-zero points were corrected by means of the pulser peaks which were recorded in all spectra together with the *n-d* data. Also, each TOF was corrected for walk as explained earlier. All additional distorting effects were included in the Monte Carlo simulations of the experiments [23,24].

In the a_{nn} experiment, the most important one was, of course, the efficiency of the *n* detector which was taken from the renormalized PTB calculations as described in Sec. II D. The *r* dependence of ε was taken into account explicitly, thereby increasing the simulated count rate in the FSI peak by 3.0%. This is a consequence of the fact that the efficiency is higher in the center of the *n* detector where, because of the more favorable kinematical circumstances, the breakup cross section is larger. Besides the extended geometry, other effects included the energy spread of the beam, the time resolution, straggling and energy loss of the protons, and the loss of neutrons due to scattering which, however, was only about 2%. Owing to the high count rate in the *n* detector, there was a probability of around 2% for any TOF in the neutron arm to be stopped early by an accidental count, thus leading to an apparent loss of true coincidences by moving the event to the left on the time axis, towards and into the ''accidentals region'' which consequently becomes somewhat contaminated by true coincidences. Based on the measured distribution of pulser counts along the TOF$_n$ axis, the exact magnitude of the necessary correction was calculated for each event. The number of recorded pulser coincidences also served to determine the overall dead time losses which were 1.8%.

For the 25.3-MeV data, another significant correction was required because of the special geometry of this experiment: since the neutron detector was positioned on the recoil axis of the $2n$ system with zero relative energy, there was a considerable probability for *both* neutrons to hit the detector. This increases the effective detection efficiency and also distorts the TOF$_n$ spectrum to some extent because the faster of the two neutrons, if detected, always determines the measured time of flight. The resulting increase of the count rate in the FSI peak was about 18%. However, even though this is a sizable effect, it is governed by simple three-body kinematics and thus depends only on the well-known geometry of the experiment. Therefore it can be calculated very accurately and was taken into account in the MC simulations for each value of a_{nn}. The ensuing additional uncertainty is very small and is included in the errors quoted in Table I. For the LE data at 16.6 MeV, where the detectors were not exactly on the recoil axis, the corresponding increase in the count rate was only 5%. There were essentially no double hits in the QFS peaks.

For the data of the a_{np} measurement the most important correction—apart from the efficiency of the *n* detectors—was due to multiple scattering in the target scintillator. The ensuing loss of neutrons was calculated using the total cross sections for carbon and deuterium. Altogether, these losses

TABLE I. Individual contributions[a] to the total error of a_{nn} deduced from the absolute yield in the FSI peak.

Source of error	Size of error	Δa_{nn} (fm)
Statistics	1.8%	0.27
Efficiency *n* detector	1.4%	0.20
Neutron beam fluence	1.1%	0.15
Target position *x*, *y*, *z*	1 mm	0.08
Solid angle *n* detector	0.9%	0.06
Solid angle *p* detector	0.8%	0.06
Gas target density	3.6%	0.04
PRT	0.3%	0.04
$\Delta\Theta_p$	0.04°	0.04
$\Delta\Theta_a$	0.06°	0.02
ΔE_0	50 keV	0.02
Other		0.06
Total error (one standard deviation)		± 0.40 fm

[a]Where applicable, the quoted errors include the effect of double hits in the *n* detector.

were of the order of 56%. However, by simulating the effects of double scattering individually it was found that 6.7% of those events which scattered *before* the breakup reaction actually did contribute to the count rate in the FSI peak, thereby increasing it by 2.6%. Also taken into account explicitly was the possibility that one of the breakup neutrons, being first emitted in an arbitrary direction, might be detected after scattering in the target; this effect amounted to a correction of +3.8%. These numbers show that double scattering must be investigated carefully in such experiments and cannot, in general, be treated summarily.

Absolute theoretical spectra were produced with $3N$ breakup cross sections obtained from rigorous, fully charge-dependent Faddeev-type calculations in momentum space using the CD-Bonn potential [20] as input for the nucleon-nucleon interaction. A detailed description of the theoretical formulation and numerical procedure can be found in Refs. [8,25,26] and will not be repeated here. The CD-Bonn interaction is charge dependent in the isospin $t=1$ states, taking the difference in the $^1S_0$ force components of the *n-n* and *n-p* subsystems explicitly into account. This potential is ''realistic'' in describing the existing $2N$ data with a normalized $\chi^2 \approx 1$. For the purpose of this analysis, modifications of the $^1S_0$ interactions were induced by adjusting one of the parameters for the fictitious σ boson in this partial wave [27], thus generating interactions with different *n-n* and *n-p* scattering lengths. For these, point-geometry cross sections were calculated for energies from 13 to 23 MeV in steps of 1 MeV and from 23 to 28 MeV in steps of 0.5 MeV, and stored in the computer. For each simulated event, the cross section was interpolated from this library and incorporated into the Monte Carlo routine. It was assured that the interpolated cross section in no case deviated from the exact value by more than 0.1%. Finally, the measured number of counts in the FSI peak was compared with the corresponding predicted numbers to find the best-fit value for the respective scattering length.

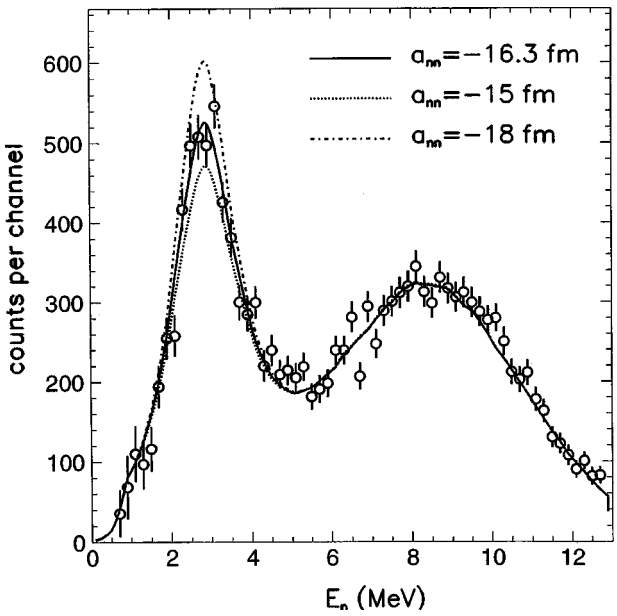

FIG. 6. The 25.3-MeV data for the *n-n* FSI (circles with error bars), after conversion of the neutron TOF into energy and projection onto the E_n axis, together with the finite-geometry Monte Carlo predictions for $a_{nn}=-15.0$, -16.3, and -18.0 fm. The narrow peak at $E_n=2.8$ MeV is due to the *n-n* FSI, the broader one at higher energies comes from *n-p* QFS.

III. RESULTS

A. *n-n* scattering length

1. Absolute cross sections

The final data at $E_0=25.3$ MeV are shown in Fig. 6, after conversion of the neutron TOF into energy and projection onto the E_n axis; a threshold of 6 MeV has been applied in E_p. Included are the finite-geometry Monte Carlo spectra calculated with $a_{nn}=-15$ fm, $a_{nn}=-16.3$ fm, and $a_{nn}=-18$ fm. Clearly, the theory agrees well with the data in the region of *n-p* QFS, both in shape and in the absolute magnitude. This is in marked contrast to our previous investigation [11] where the calculations were based on a crude finite-rank approximation for the *NN* interaction. In order to extract the *n-n* scattering length, a minimum-χ^2 fit was made to the FSI peak which resulted in a value of

$$a_{nn}=-16.27\pm 0.40 \text{ fm}.$$

For this fit, the absolute yield in the region between $E_n=1.5$ and 4.5 MeV was compared with the MC predictions for different values of a_{nn}. The range of comparison was optimized for maximum sensitivity with regard to a_{nn}. Data points at lower energies were excluded from the fit because, at a bias of 60 keV ee, the efficiency of the *n* detector depends too much on the resolution and threshold below 1.5 MeV. The shape of the FSI peak is well reproduced by the simulation, with $\chi^2_{\min}=32$ for 28 degrees of freedom (Fig. 7). The best fit was obtained when the simulated spectra were shifted by 70 keV with respect to the measured one, the

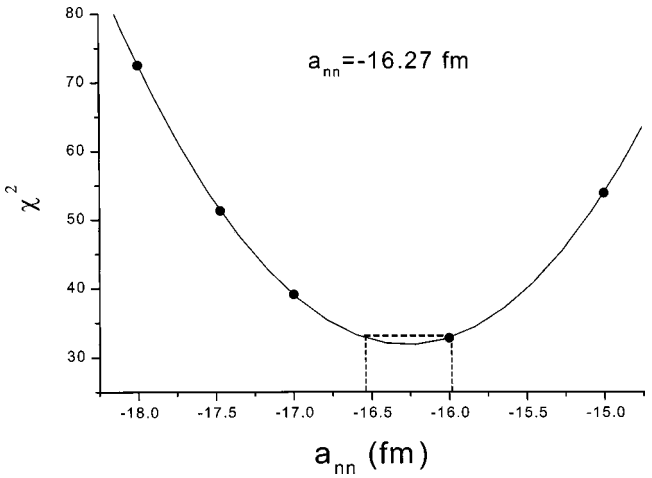

FIG. 7. χ^2 vs a_{nn} for the fit to the absolute yield in the *n-n* FSI peak between $E_n = 1.5$ MeV and $E_n = 4.5$ MeV. Indicated are the values of a_{nn} at $\chi^2_{\min}+1$.

reason being an imperfect walk correction in TOF_n. However, the change in a_{nn} caused by this shift was only 0.03 fm.

The influence of the various experimental uncertainties on the result for a_{nn} was also investigated by means of Monte Carlo simulations; the important contributions are listed in Table I together with the total error which ensues from adding all statistical and systematic errors quadratically. Changing the threshold in the *n* detector to 40 keV ee and the energy range of the fit to $1.0 \leqslant E_n \leqslant 5.0$ MeV moved the best-fit value of a_{nn} to -16.33 fm.

In order to facilitate a possible reanalysis of our experiment, the point-geometry cross sections are shown in Fig. 8,

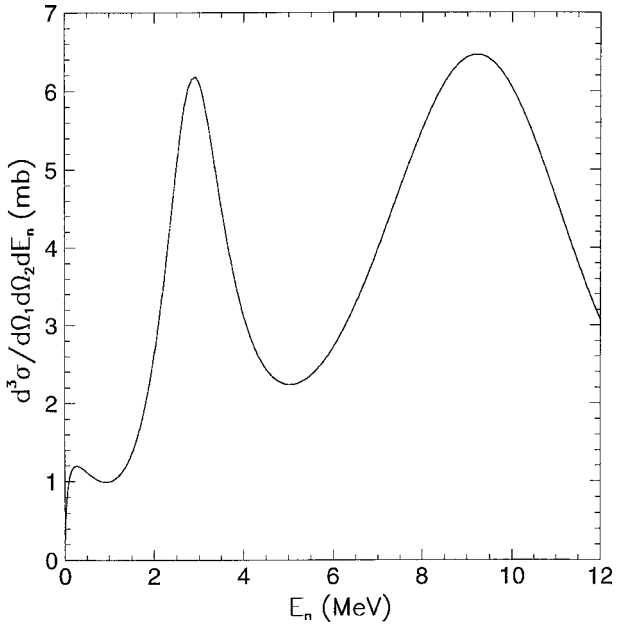

FIG. 8. Theoretical point-geometry cross section for the $^2\mathrm{H}(n,np)n$ reaction, calculated with CD Bonn for $E_0 = 25.5$ MeV and $a_{nn} = -16.3$ fm, at $\Theta_n = 55.5°$, $\Theta_p = 41.15°$, and $\Theta_{np} = 180°$. The relative suppression of the QFS peak in the real data (Fig. 6) is primarily caused by the efficiency of the *n* detector.

TABLE II. Calculated (CD-Bonn) point-geometry cross sections (mb/sr^2 MeV) for $E_0 = 25.5$ MeV and $a_{nn} = -16.3$ fm, at $\Theta_n = 55.5°$, $\Theta_p = 41.15°$, and $\Phi_{np} = 180°$. S is the arc length of the kinematical locus, defined in the usual way [8].

E_n (MeV)	$d^3\sigma/d\Omega_n\, d\Omega_p\, dE_n$	S (MeV)	$d^3\sigma/d\Omega_n\, d\Omega_p\, dS$
1.0	1.00	19.0	3.05
1.5	1.36	20.0	3.80
2.0	2.62	21.0	4.36
2.5	5.00	21.8	4.52[b]
2.9	6.21[a]	23.0	4.19
3.5	4.53	24.0	3.49
4.0	3.14	25.0	2.70
4.5	2.45	26.0	2.11
5.0	2.23	26.5	1.99
5.5	2.35	27.0	2.06
6.0	2.71	27.5	2.42
7.0	3.98	28.0	3.27
8.0	5.51	28.5	4.84
9.2	6.47[b]	29.0	6.21[a]
10.0	6.06	29.5	4.45
11.0	4.63	30.0	2.14
12.0	3.09	30.5	1.08
13.0	2.26	31.0	0.68

[a]Denotes the maximum of the *n-n* FSI peak.
[b]Denotes the maximum of the *n-p* QFS peak.

calculated with CD Bonn without three-nucleon forces, for $E_0 = 25.5$ MeV and $\Theta_n = 55.5°$, $\Theta_p = 41.15°$, and $\Phi_{np} = 180°$, with $a_{nn} = -16.3$ fm which is that value of the scattering length which best describes our absolute data (see Fig. 6). This curve can thus be seen as a quantitative representation of our ''unfolded'' data, with all experimental effects removed, which may directly be compared to other theoretical calculations. Individual values for the cross section are listed in Table II, both as a function of E_n and S, the arc length of the kinematical locus as defined in Ref. [8].

2. Relative cross sections (HE)

Since in the region of *n-p* QFS the cross section is practically independent of a_{nn}, it provides an intrinsic normalization for the FSI peak. Using for this the data between $E_n = 5$ and 12 MeV, the normalization factor is 0.984 ± 0.012. Performing the analysis with the data between 1.5 and 4.5 MeV renormalized in this way, we obtain

$$a_{nn} = -16.06 \pm 0.35 \text{ fm}.$$

Of course, since the normalization factor is close to 1, this value for a_{nn} does not differ much from the one obtained by fitting the absolute yield. However, the sources of errors for the two results are quite different. The error here is mainly caused by statistics while most systematic errors have canceled out.

3. Relative cross sections (LE)

As explained in Sec. II C, an accurate *absolute* calibration was only performed for the HE part of the *n* beam. However,

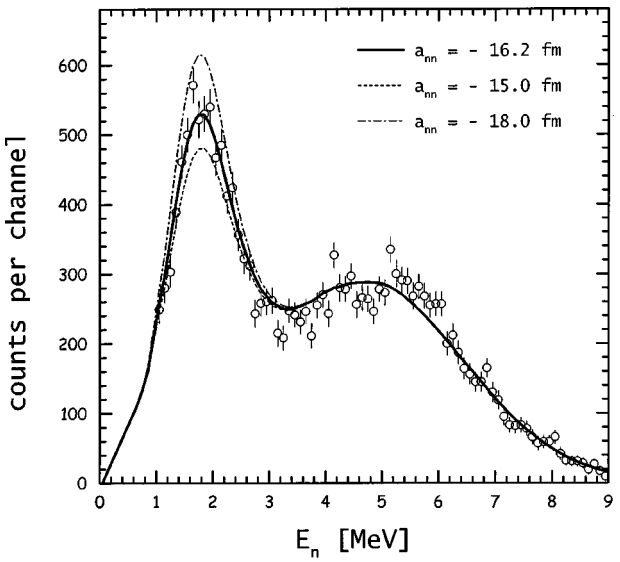

FIG. 9. The 16.6 MeV data for the *n-n* FSI, projected onto the E_n axis, together with the finite-geometry Monte Carlo predictions for $a_{nn}=-15.0$, -16.2, and -18.0 fm. The data were normalized to the Monte Carlo calculation in the region of *n-p* QFS between $E_n=3.4$ and 9.0 MeV.

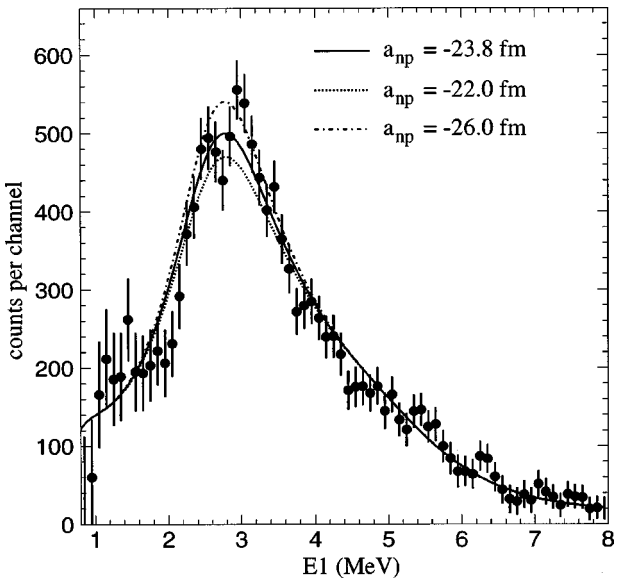

FIG. 10. The data for the *n-p* FSI (1–3) after conversion of the neutron TOF into energy and projection onto the E_{n1} axis, together with the finite-geometry Monte Carlo predictions for $a_{np}=-23.8$, -22.0, and -26.0 fm.

the upper part of the LE neutrons could be employed for an analysis based on the comparison of *relative* count rates. For this, a window was set in TOF_C to select neutrons with an average energy $E_0=16.6$ MeV and a full width at half maximum $\Delta E_0=3.0$ MeV. The energy distribution of this part of the LE beam was obtained from a Monte Carlo simulation based on the spectral shape of the breakup continuum as measured with the PRT. Normalizing then the data in the *n-p* QFS region between $E_n=3.4$ and 9.0 MeV to the corresponding theoretical prediction, the minimum-χ^2 fit to the *n-n* FSI peak between 1.1 and 2.7 MeV yields

$$a_{nn}=-16.16\pm0.34\,\mathrm{fm}$$

(Fig. 9), with $\chi^2_{\min}/\mathrm{d.o.f.}=1.0$. This result is obtained with thresholds of 2 MeV in the *p* detector and 40 keV ee in the *n* detector, respectively. At 0.24 fm, the main contribution to the total error is due to statistics while the specific choice of the boundaries for the fit and for the normalization region produces an additional error of up to 0.16 fm. The uncertainty in the exact energy distribution of the neutron beam contributes 0.08 fm while all remaining effects add up to 0.16 fm.

B. *n-p* scattering length

In the a_{np} measurement there are two regions of phase space where the FSI can be observed: one between the particles n_1 and *p*, which kinematically corresponds to the *n-n* FSI discussed in the previous section (see Fig. 1), and another one between n_2 and *p*. The results are depicted in Figs. 10 and 11, where the data are shown projected onto the respective E_n axis, together with the finite-geometry MC simulations for three values of a_{np}. There are no peaks from QFS in these spectra since most spectator protons do not produce a signal in the target scintillator. Therefore the *n-p* scattering length could only be determined through the *absolute* yield in the FSI peaks, utilizing the HE part of the beam.

The results of the minimum-χ^2 fits were $a_{np}=-23.8\pm1.1$ fm for the n_1-*p* FSI (with $\chi^2_{\min}/\mathrm{d.o.f.}=1.2$), and $a_{np}=-24.0\pm1.4$ fm for the n_2-*p* FSI (with $\chi^2_{\min}/\mathrm{d.o.f.}=1.3$); combining the two we obtain

$$a_{np}=-23.9\pm1.0\,\mathrm{fm}.$$

The error consists to approximately equal parts of statistical and systematic uncertainties, both of which are larger here

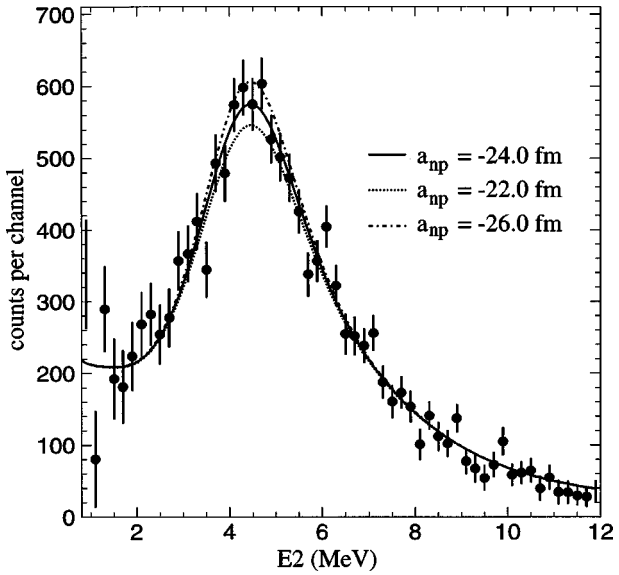

FIG. 11. Same as Fig. 10, but for the *n-p* FSI (2–3), projected onto the E_{n2} axis, with the predictions for $a_{np}=-24.0$, -22.0, and -26.0 fm.

than in the a_{nn} measurement because the dependence of the cross section on the scattering length is significantly smaller in the case of a_{np}, and there was a larger accidental background. Obviously, within the error bar, there is very good agreement between our result and the accurately known value obtained from free *n-p* scattering, which is -23.748 ± 0.009 fm [28].

IV. DISCUSSION

The outcome of this experiment is puzzling. With an average of -16.2 ± 0.3 fm, our result for a_{nn} clearly disagrees with the findings of a similar investigation performed at TUNL (Durham, NC) in a ''final-state'' geometry, which yielded $a_{nn} = -18.7 \pm 0.6$ fm [10]; the results of the two experiments differ by almost four standard deviations. Our result is also at variance with the average value from the $^2\mathrm{H}(\pi^-, nn)\gamma$ reaction, which now is -18.6 ± 0.4 fm [29–31]. On the other hand, all values obtained from the present experiment agree very well among each other, and it must be emphasized that they represent three largely self-contained results: the only major uncertainty which affects both of our HE results is the statistical error in the FSI peak, and the LE value is essentially independent of the two HE results. This makes it highly unlikely that systematic errors are to blame for the observed disagreement, and statistics definitely cannot explain it either. Furthermore, our results agree with those of all other kinematically complete, *n*-induced breakup experiments (see Ref. [5]), irrespective of the type of reaction or kind of analysis used to extract a_{nn}, and it should be recalled that these older results cannot be dismissed simply because they were obtained with less sophisticated theoretical methods, as was pointed out in Sec. I; the maximum possible error introduced by the use of more simplified models is at least a factor of 4 smaller than the discrepancy at issue. Finally, as detailed in Ref. [9], neither the use of different *NN* potentials [18,19] in the Faddeev calculations nor the inclusion of the Tucson-Melbourne (TM) 2π-exchange three-nucleon force [32] produces noticeably different results.

Conversely, the neutron-proton FSI was observed in the *same* geometry at TUNL [10] and in the present experiment. In both cases the angles were chosen according to the prescription of Witala *et al.* [9], and the neutron from the FSI pair was detected in coincidence with the recoiling neutron on the opposite side of the beam. Perhaps not surprisingly, both experiments yielded the same result for a_{np}, in perfect agreement with the known value from free *n-p* scattering. One is therefore led to speculate that the observed discrepancy with respect to a_{nn} might have something to do with the specific configuration in which the FSI was observed. A direct test of this would be to measure a_{np} using the ''final-state'' geometry, i.e., detecting the neutron and the proton at the same angle on one side of the beam. Actually, one such experiment has already been done, albeit employing a different reaction: Bodek *et al.* [33] have investigated the *n-p* FSI in this way in the $^9\mathrm{Be}(p,np)^8\mathrm{Be}$ reaction and got $a_{np} = -23.8 \pm 1.2$ fm. Although this result was obtained with a simple Watson-Migdal analysis, it is valid nevertheless, as stated before. However, it only proves that the *shape* of the FSI peak does not depend on the geometry of the experiment.

TABLE III. Survey of the (average) values of a_{nn} and a_{np} obtained in different experimental geometries by analyzing either the shape of the FSI peak or the cross section. ''Recoil'' indicates that one of the FSI partners was detected in coincidence with the recoiling particle on the other side of the beam, while ''final state'' means that both FSI particles were detected at (nearly) the same angle on one side of the beam. The value of a_{np} from free *n-p* scattering is -23.748 ± 0.009 fm [28].

Experimental geometry and type of analysis	a_{nn} (fm)	a_{np} (fm)
recoil and shape	-16.8 ± 0.5[a]	-23.6 ± 0.2[b]
recoil and cross section	-16.2 ± 0.3[c]	-23.7 ± 0.6[c,d]
final state and shape	-16.8 ± 0.3[e]	-23.8 ± 1.1[f]
final state and cross section	-18.7 ± 0.6[d]	?

[a]References [11,37].
[b]Average of values listed in Ref. [36].
[c]Average of this paper.
[d]Reference [10].
[e]Average of values listed in Refs. [5,40].
[f]Reference [33].

The result of Ref. [33] also shows that the possible influence of three-body (or Coulomb) force effects on the *shape* must be small since all comparable investigations in the much lighter *p-d* system[1] have consistently yielded the same result for a_{np} [4,35,36]. The absence of significant 3BF effects on the *cross section*, already observed in Ref. [10], is also supported by our own results: as the production angle for the n_2-*p* pair is around 41°, it is far enough removed from the ''magic'' angle of 55.5° to produce a predicted change of +3.3% in the cross section if the TM 3BF is included. This in turn should lead to a change of +1.3 fm in a_{np} if the 3BF were wrongly ignored. However, our results do not show such a shift. Although this is only a 1σ effect in our case, it corroborates the findings of Ref. [10] which clearly speak against the presence of any appreciable 3BF effects in this reaction. This implies, of course, that the present-day three-body forces, like the TM 3BF, which do predict detectable effects, are not realistic.

The situation at present is summarized in Table III where the (average) values of a_{nn} and a_{np} are listed as obtained through kinematically complete, *n*- or *p*-induced breakup reactions, respectively, using either the ''recoil'' or the ''final-state'' geometry. All experiments in which the *shape* of the FSI peak was used to extract the scattering length gave consistent results which, in the case of a_{np}, agree very well with the known value from free *n-p* scattering. Our values for a_{nn}, deduced from both absolute and relative cross sections, agree with those obtained via shape analysis while Ref. [10], obtained in final state geometry, disagrees. Unfortunately,

[1]The influence of the Coulomb force on the *n-p* FSI cross section was also found to be very small in Ref. [34].

there is no analog result for a_{np} to serve as a check in this case. Although it is not obvious why the geometry should make any difference, it is interesting to note that the theoretical cross sections for the two configurations—at the *same* energy and production angle for the *n-n* pair, and for the *same* value of a_{nn}—differ by a factor of 4 and there is the possibility that the prediction for the cross section in the final state geometry might be wrong. There are other kinematical situations where this is the case, most notably the so-called ''space star'' geometry where the measured *n-d* breakup cross sections are 25% higher than the predicted ones [38]. Another hint in this direction comes from the reanalysis [7] of kinematically incomplete experiments with modern three-body calculations which revealed similar deviations in certain parts of the spectra [39]. Thus inspection of Table III suggests that the cross section of the *n-d* breakup reaction in the final-state geometry might not be a suitable tool for the extraction of a_{nn}, and the missing test regarding a_{np} should urgently be performed. There remains, of course, the additional question why most experiments using the ^{2}H$(\pi^-,nn)\gamma$ reaction have provided a result for a_{nn} which is at variance with exactly those *n-d* values which *have* been cross checked against a_{np}.

V. SUMMARY

The neutron-neutron and neutron-proton final-state interactions have been investigated at 25.3 MeV in two kinematically complete experiments using the *n-d* breakup reaction. In both experiments, absolute cross sections were measured in the same geometry, detecting one of the participating FSI particles in coincidence with the corresponding recoil particle on the other side of the beam. For the *n-n* FSI, relative cross sections were also studied at 16.6 MeV. The angles were chosen such as to allow, in theory, an essentially model-independent extraction of the $^1S_0$ scattering lengths a_{nn} and a_{np}, respectively. The analysis was performed by means of sophisticated Monte Carlo simulations based on rigorous three-body calculations using the CD-Bonn potential as input for the nucleon-nucleon interaction, with or without addition of the Tucson-Melbourne three-body force.

Our results for a_{nn} differ dramatically from those of a similar investigation done at TUNL at 13 MeV in which a different geometry was employed. They also disagree with the average value obtained through the ^{2}H$(\pi^-,nn)\gamma$ reaction. They agree, however, among themselves and with the results of all other kinematically complete, *n*-induced breakup experiments. Regarding a_{np}, our own experiment and all other experiments performed to date have consistently reproduced the well-known result from free *n-p* scattering, suggesting that the *n-d* reaction is basically a reliable tool for the extraction of a_{nn}. However, for each particular experiment the result should be verified by way of comparison with an analog measurement of a_{np}, performed in the *same* geometry. Finally, at the present level of accuracy, there is no evidence for the action of three-body forces in the *n-p* or *n-n* final-state interaction at low bombarding energies.

ACKNOWLEDGMENTS

The authors wish to thank I. Fabry and P. Hilger for their help during parts of the experiment. This work was supported in part by the Deutsche Forschungsgemeinschaft under Grant Nos. WI 1144/5-1 and WI 1144/5-2, and by the Polish Committee for Scientific Research under Grant No. 2P03B02818. The numerical calculations were performed on the CRAY T90 and T3E of the John von Neumann Institute for Computing in Jülich, Germany.

[1] D. Y. Wong and H. P. Noyes, Phys. Rev. **126**, 1866 (1962).
[2] G. A. Miller, B. M. K. Nefkens, and I. Šlaus, Phys. Rep. **194**, 1 (1990).
[3] B. Kühn, Fiz. Elem. Chastits At. Yadra [Sov. J. Part. Nucl. **6**, 139 (1976)].
[4] D. R. Tilley, H. R. Weller, and H. H. Hasan, Nucl. Phys. **A474**, 1 (1987), and references therein.
[5] K. Bodek, J. Krug, W. Lübke, S. Obermanns, H. Rühl, M. Steinke, M. Stephan, and D. Kamke, Few-Body Syst. **8**, 23 (1990), and references therein.
[6] K. M. Watson, Phys. Rev. **88**, 1163 (1952); A. B. Migdal, Zh. Eksp. Teor. Fiz. **28**, 3 (1956) [Sov. Phys. JETP **1**, 2 (1955)].
[7] W. Tornow, R. T. Braun, and H. Witała, Phys. Lett. B **318**, 281 (1993); W. Tornow, H. Witała, and R. T. Braun, Few-Body Syst. **21**, 97 (1996).
[8] W. Glöckle, H. Witała, D. Hüber, H. Kamada, and J. Golak, Phys. Rep. **274**, 107 (1996).
[9] H. Witała, D. Hüber, W. Glöckle, W. Tornow, and D. E. González Trotter, Few-Body Syst. **20**, 81 (1996).
[10] D. E. Gonzáles Trotter, F. Salinas, Q. Chen, A. S. Crowell, W. Glöckle, C. R. Howell, C. D. Roper, D. Schmidt, I. Šlaus, H. Tang, W. Tornow, R. L. Walter, H. Witała, and Z. Zhou, Phys. Rev. Lett. **83**, 3788 (1999).
[11] W. von Witsch, B. Gómez Moreno, W. Rosenstock, and K. Ettling, Nucl. Phys. **A329**, 141 (1979).
[12] M. Hohlweck, T. Köble, F. Meyer, M. Ockenfels, J. Weltz, and W. von Witsch, Nucl. Instrum. Methods Phys. Res. A **281**, 277 (1989).
[13] Supplied by Nuclear Enterprises Technology Limited, Edinburgh, Scotland.
[14] P. Hempen, P. Clotten, K. Hofenbitzer, T. Köble, W. Metschulat, M. Schwindt, W. von Witsch, L. Wätzold, J. Weltz, W. Glöckle, D. Hüber, and H. Witała, Phys. Rev. C **57**, 484 (1998).
[15] Supplied by Bicron Corporation, Newbury, Ohio.
[16] V. G. J. Stoks, R. A. M. Klomp, M. C. M. Rentmeester, and J. J. de Swart, Phys. Rev. C **48**, 792 (1993).
[17] R. A. Arndt, I. Strakovsky, and R. L. Workman, Phys. Rev. C **50**, 2731 (1994); R. A. Arndt, Interactive computer code SAID; (private communication).
[18] V. G. J. Stoks, R. A. M. Klomp, C. P. F. Terheggen, and J. J. de Swart, Phys. Rev. C **49**, 2950 (1994).

[19] R. B. Wiringa, V. G. J. Stoks, and R. Schiavilla, Phys. Rev. C **51**, 38 (1995).
[20] R. Machleidt, F. Sammarruca, and Y. Song, Phys. Rev. C **53**, 1483 (1996).
[21] I. Fabry, Diploma thesis, University of Bonn, 1998.
[22] G. Dietze and H. Klein, Technical Report No. PTB-ND-22, 1982, Physikalisch-Technische Bundesanstalt Braunschweig, Germany; G. Dietze and H. Klein, Nucl. Instrum. Methods Phys. Res. **193**, 549 (1982).
[23] V. Huhn, Diploma thesis, University of Bonn, 1995; Ph.D. thesis, University of Bonn, 2000.
[24] Ch. Weber, Diploma thesis, University of Bonn, 1995; Ph.D. thesis, University of Bonn, 2000.
[25] H. Witała, Th. Cornelius, and W. Glöckle, Few-Body Syst. **3**, 123 (1988).
[26] H. Witała, W. Glöckle, and Th. Cornelius, Phys. Rev. C **39**, 384 (1989).
[27] R. Machleidt, Adv. Nucl. Phys. **19**, 189 (1989).
[28] L. Koester and W. Nistler, Z. Phys. A **272**, 189 (1975).
[29] C. R. Howell *et al.*, Phys. Lett. B **444**, 252 (1998).
[30] O. Schori, B. Gabioud, C. Joseph, J. P. Perroud, D. Rüegger, M. T. Tran, P. Truöl, E. Winkelmann, and W. Dahme, Phys. Rev. C **35**, 2252 (1987).
[31] B. Gabioud *et al.*, Nucl. Phys. **A420**, 496 (1984).
[32] S. A. Coon, M. D. Scadron, P. C. McNamee, B. R. Barrett, D. W. E. Blatt, and B. H. J. McKellar, Nucl. Phys. **A317**, 242 (1979); S. A. Coon and W. Glöckle, Phys. Rev. C **23**, 1790 (1981).
[33] K. Bodek, B. Brüggemann, J. Krug, P. Lekkas, W. Lübke, H. Rühl, M. Steinke, M. Stephan, A. Szczurek, and D. Kamke, Few-Body Syst. **3**, 135 (1988).
[34] E. O. Alt and M. Rauh, Few-Body Syst. **17**, 121 (1994).
[35] A. Niiler, C. Joseph, V. Valkovic, W. von Witsch, and G. C. Phillips, Phys. Rev. **182**, 1083 (1969).
[36] I. Šlaus, in *Three Body Problem in Nuclear and Particle Physics*, Birmingham, 1969, edited by J. S. C. McKee and P. M. Rolph (North-Holland, Amsterdam, 1970), p. 350.
[37] M. W. McNaughton, R. J. Griffiths, I. M. Blair, B. E. Bonner, J. A. Edgington, M. P. May, and N. M. Stewart, Nucl. Phys. **A239**, 29 (1975).
[38] C. R. Howell *et al.*, Nucl. Phys. **A631**, 692c (1998), and references therein.
[39] W. Tornow, R. T. Braun, H. Witała, and N. Koori, Phys. Rev. C **54**, 42 (1996).
[40] W. Lübcke, Ph.D. thesis, University of Bochum, 1992.